# STUDY OF THE AC CONDUCTANCE MECHANISM OF EVAPORATED AMORPHOUS SILICON FILMS

by

AYHAN O. GÜLSOY

Submitted to the Institute for Graduate Studies in Science and Engineering in partial fulfilment of the requirements for the degree of

Master of Science

in

ELECTRICAL ENGINEERING



Boğaziçi University

1986

ACKNOWLEDGEMENTS

I would like to express my sincere gratitude to my thesis supervisor Y. Doç. Dr. Gülen AKTAŞ for her guidance, encouragement and invaluable suggestions during my study.

I would like to thank Prof. Dr. Yani SKARLATOS for the preparation of the films and his valuable suggestions.

## ABSTRACT

In this thesis AC (and DC) bulk characteristics of amorphous silicon films are investigated. The films were prepared by electron gun evaporation in a conventional vacuum system. Ohmic contacts were established between the silicon films and the aluminium electrodes. I-V and I-T measurements were performed in the temperature range, 77°K to 400°K. Room temperature measurements showed that the preparation conditions such as evaporation rate and subsequent annealing affect the electrical properties of the films. Conductivity versus frequency measurements were performed in the frequency range, 100 Hz to 1 MHz. In the low temperature range, the data analyzed with the existing AC and DC models of amorphous semiconductors and the density of states near the Fermi level was calculated. The high temperature data were used to calculate the mobility gap of the amorphous silicon films. The results were then compared with the previously published work.

# ÖZETÇE

Bu çalışmada, vakumda buharlaştırma yöntemiyle hazırlanan amorf silisyum filmlerin alternatif akım (ve doğru akım) gövde karakteristikleri incelenmiştir. Alüminyum elektrodlar ile silisyum filmler arasındaki kontağın omik olduğu gözlenmiştir. Filmlerin I-V ve I-T ölçümleri 77°K ile 400°K sıcaklık aralığında alınmış olup, oda sıcaklığı dolayındaki ölçümlerde hazırlama koşullarının filmlerin elektriksel özelliklerini nasıl etkilediği araştırılmıştır. İletkenliğin frekansa bağımlılığı ölçümleri 100 Hz ile 1 MHz frekans aralığında yapılmıştır. Düşük sıcaklıklarda elde edilen veriler var olan amorf silisyum modellerinin ışığı altında incelenmiş ve Fermi sevisindeki durum yoğunluğu hesaplanmıştır. Yüksek sıcaklıklardaki verilerden ise amorf silisyum filmlerin iletkenlik bandı hesaplanmıştır. Elde edilen sonuçlar diğer araştırmacıların sonuçları ile karşılaştırılmıştır.

TABLE OF CONTENTS

# LIST OF FIGURES

FIGURE 3.7 The Variation of Conductivity as a Function of $T^{-1/4}$ of Sample 17.11.85-I

FIGURE 3.8 The Variation of Conductivity as a Function of $T^{-1/4}$ of Sample 27.III.86-I

FIGURE 3.9 Frequency Dependence of the Conductivity at the Indicated Temperatures

FIGURE 3.10 Frequency Dependence of the Conductivity at the Indicated Temperatures

FIGURE 3.11 DC Conduction Plotted Against The Density of States at the Fermi level Determined a) From variable range hopping DC data and b) From AC Conduction measurements on the same samples

# INTRODUCTION

Since 1960's amorphous semiconductors have become one of the major research topics of both theoretical and experimental solid state physics. The rapid development in the semiconductor technology during the last two decades with the hope that crystalline semiconductors would be replaced by amorphous semiconductors, which are cheaper to produce, have attracted the interest of many researchers and the number of articles published on this subject has increased at an enormous rate.

The term amorphous is used for materials prepared in the form of a thin film on a relatively cold substrate to prevent crystallization.

The aim of this work is to investigate the AC (and DC) characteristics of amorphous silicon films prepared by evaporation in order to gain a better understanding of the bulk properties.

In the first chapter, a general theory about the structure of amorphous silicon and the temperature and frequency dependences of the conductivity are given. The second chapter gives the technique of preparation of the films and the set-up used in AC and DC measurements. In the third chapter the results are given and are analyzed in terms of the electrical properties of the films. The results are discussed in comparison with the results of other researchers.

# I. THEORY

## 1.1 STRUCTURE OF AMORPHOUS SOLIDS

With crystalline materials, one first characterizes the ideal periodic structure with a determination of the short-range coordination and through a knowledge of the translational symmetry the long-range order. Further characterization then involves the determination of the concentration various types of defects and impurities as deviations from the ideal structure.

X-ray diffraction experiments have shown that an amorphous material has a good short range order; the positions of the nearest neighbours being essentially the same as in the crystalline materials. But an amorphous material unlike a crystal has no long-range order so at a distance far from the atom in question the other atoms appear to be randomly distributed. This type of disorder is a positional disorder. There are also structural disorders in amorphous semiconductor films and these are voids and dangling bonds. In fact, in the amorphous materials there is no ideal structure which can be accepted with full confidence.

The previous research on amorphous materials shows that the electrical and optical properties of amorphous films depend strongly on the preparation methods. (1, 2) There are three basic preparation methods for amorphous silicon films. These are:

1- Vacuum evaporation
2- Sputtering
3- Glow-discharge decomposition of silane ($SiH_4$)

The specimens prepared by glow-discharge decomposition of silane have fewer voids and dangling bonds compared to those prepared by evaporation or sputtering techniques. (3, 4)

This is assumed to be caused by the presence of hydrogen during deposition tending to saturate the dangling bonds. The films are structurally heteregeneous when they are deposited on a cold substrate, by evaporation or sputtering. They contain a network of internal voids and dangling bonds.

Because of the extensive disorder present, the Bloch theorem, does not hold for amorphous semiconductors and hence many of the results derived for crystals do not apply directly to amorphous solids. In particular, the concept of the wave vector $\vec{k}$, characterizing the electron wave function, is no longer meaningful. This is also true for the k - space and Brillouin zones. These concepts, which are directly consequences of the translational periodicity of a crystal lattice, have to be discarded when we consider an amorphous solid. Other concepts used in connection with crystals remain useful however, even in disordered states.

In crystalline semiconductors, the impurity atoms form the impurity energy bands in the forbidden energy gap. These impurity energy levels constitute a narrow and continuous band. They constitute localized energy states like donor and acceptor energy levels closer to conduction band and valence band respectively. In the amorphous semiconductors, however, the lack of long-range order and structural defects cause a continuous distribution of localized states throughout energy gap.

Davis and Mott (1970) and Cohen, Fritzche and Ovshinsky (CFO) (1969) suggested models for the distribution of the density of localized states in order to explain the conduction mechanisms in amorphous semiconductors. (1.5) These two models are illustrated in Figure 1.1 where the shaded regions represent the localized states. In contrast to the crystal, the density of states does not vanish anywhere in the entire range of the energy gap. The density of states extends into the gap from both the conduction band (CB) and valence band (VB). The localized electron states near the

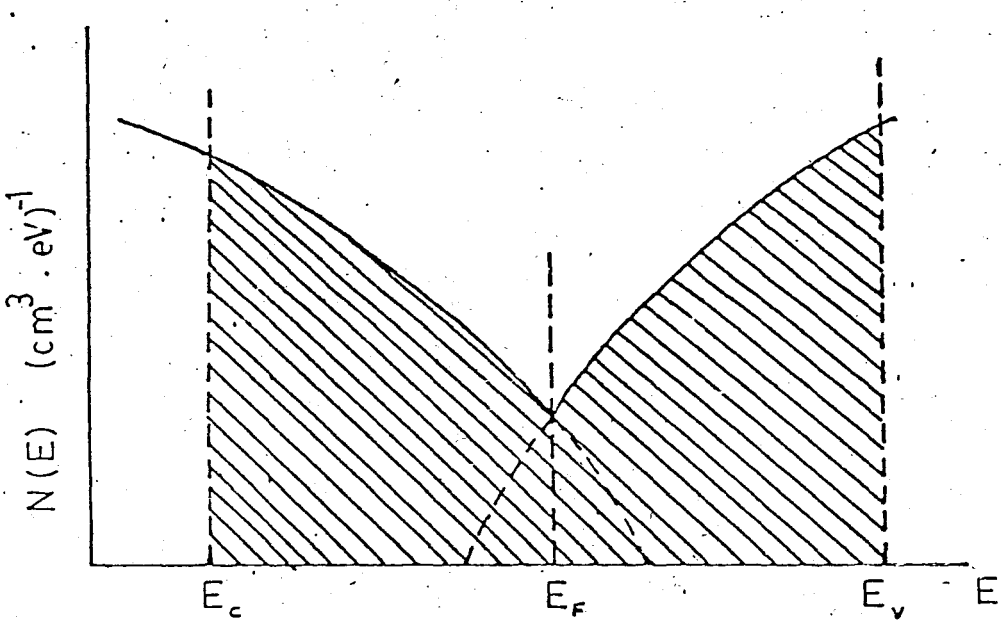


(a)

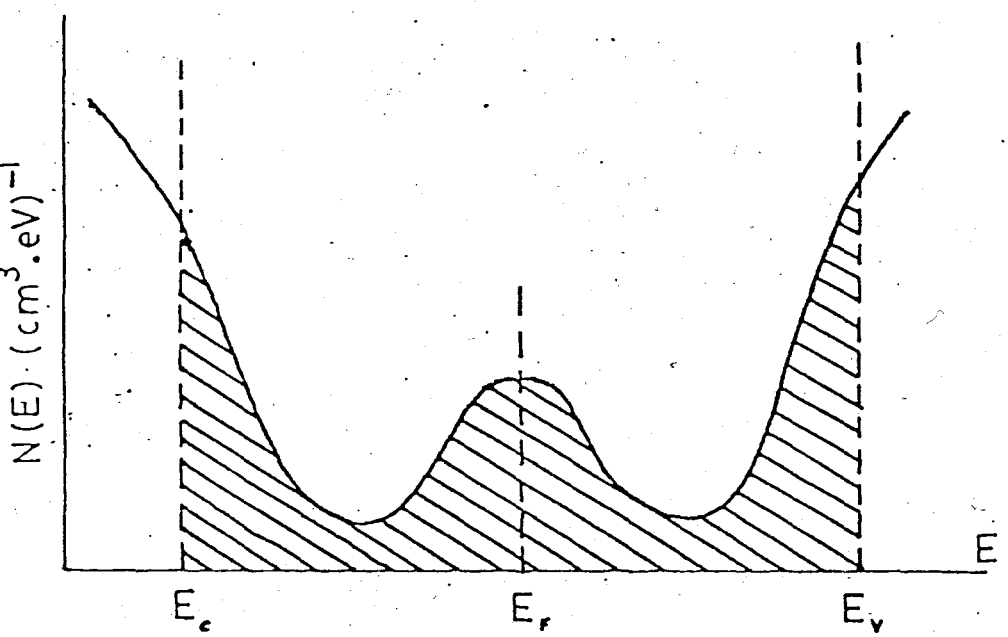


(b)

FIGURE 1.1

Models for the Distribution of the Density of Localized States

a) Cohen, Fritzche, Ovshinsky Model

(b) Davis and Mott Model

band edges are due to the lack of long-range order. The localized states near the middle of the gap are assumed to originate from the dangling bonds.

In the CFO model, tails of localized states extend from the valence and conduction bands far into the energy gap. Near the center of the gap, these states overlap. When such an overlap takes place repopulation occurs, with electrons transferring from the higher region of the valence band tail into the lower region of the conduction band tail. Since the states are localized, this results in the creation of large concentrations of positively and negatively charged centers or traps. These charged states (donor-like and acceptor-like states ) effectively pin the fermi level.

In the Davis and Mott model, the tails of localized states do not overlap. The position of the Fermi level is determined by the band of the localized states near the middle of the gap which reaches a maximum at the center and then decreases on both sides.

A common feature of these density of state models is that there is a finite density of localized states at the Fermi energy.

Due to the different character of electron states, above and below conduction band edge ($E_c$) and valence band edge ($E_v$), different conduction mechanisms are to be expected. Whereas in the extended states, charged carriers are assumed to move with an almost normal mobility of about 1 to 10 $cm^2/v.sec$, the transport in localized states can only occur by phonon assisted tunneling. (6) This is why at the transition from the extended to localized states at $E_c$ and $E_v$, the mobility drops sharply by some orders of magnitude giving rise to mobility edges. As a consequence, a pseudo gap, called the mobility gap, $E_c - E_v$ arises.

## 1.2 ELECTRICAL PROPERTIES OF AMORPHOUS SEMICONDUCTORS

The distribution of localized states in the mobility gap of amorphous semiconductors is of fundamental importance in the interpretation of their transport properties. Yet our knowledge of the state distribution N(E), even in widely studied materials is still very limited. There are various methods like field-effect, C-V, DLTS(deep level transient spectroscopy) employed in the determination of the distribution of density of states. The reliability of these methods is still controversial. (7) However, for characterizing and comparing the properties of series of amorphous specimens it is often sufficient to know the density of states at the Fermi level $N(E_f)$. There are two comparatively straightforward transport measurements which should in principle provide this information : determination of the AC conductivity, $\sigma_{AC}$ , and measurement of the temperature dependence of the DC conductivity $\sigma_{DC}$ , in the variable range hopping regime. Frequent doubts have, however, been expressed by workers in the field as to the validity of the $N(E_f)$ values deduced from either of these experiments (8).

### 1.2.1 DC Conductivity

There are two different conductivity mechanisms in amorphous semiconductors. In the extended state conduction at high temperatures, the electrons are excited to the conduction band and holes to the valence band. At low temperatures the conductivity mechanism is dominated by phonon assisted hopping in the regions of localized states.

Using the models described for the density of states in the previous section and the concept of the mobility edges in an amorphous semiconductor, one would expect three mechanisms of conduction within the mobility gap.

1. Transport by carriers excited beyond the mobility edges at $E_c$ and $E_v$, into extended states. The conductivity for electrons is,

$$\sigma = \sigma_{min} \exp\left(-\frac{(E_c - E_f)}{kT}\right) \qquad 1.1$$

where $\sigma_{min}$ is the minimum metallic conductivity given by

$$\sigma_{min} = 0.026 \frac{q^2}{\hbar} = \frac{610}{a} (\Omega - cm)^{-1}$$

where, a is the interatomic spacing and $E_f$ and $E_c$ are the Fermi energy and conduction band edge energy respectively (1, 6, 9).

2. Transport by carriers excited into the localized states at the band edges and hopping at energies ($E_1$). For this process, assuming again conduction by electrons, the conductivity is given as,

$$\sigma = \sigma_1 \exp\left(-\frac{E_1 - E_f - W_1}{kT}\right) \qquad 1.2$$

where $E_1$ is the energy level in the localized state region near the conduction band edge, $W_1$ is the activation energy for hopping at energy $E_1$, and $\sigma_1$ is the pre-exponential factor.

3. If the density of states at $E_f$ is finite, then there will be a contribution from carriers with energies

near $E_f$, which can hop between localized states. We may write for this contribution,

$$\sigma = \sigma_2 \exp\left(-\frac{W_2}{kT}\right) \qquad 1.3$$

where $W_2$ is the activation energy for hopping near the Fermi energy and $\sigma_2$ is the pre-exponential factor.

According to Mott, at very low temperatures, such as kT less than the bandwidth of the Fermi energy and for a finite density of states near the Fermi energy, the hopping will not be between nearest neighbour, but variable range hopping will take place (1,9). For this mechanism of variable range hopping the conductivity varies as,

$$\sigma = \sigma_o \exp\left(-\frac{T_o}{T}\right)^{1/4} \qquad 1.4$$

where

$$T_o = \frac{18\alpha^3}{kN(E_f)} \qquad 1.5$$

and $\alpha$ is the reciprocal of the attenuation distance of the localized wavefunction ; $N(E_f)$ is the density of localized states at $E_f$ and, k is the Boltzmann constant.

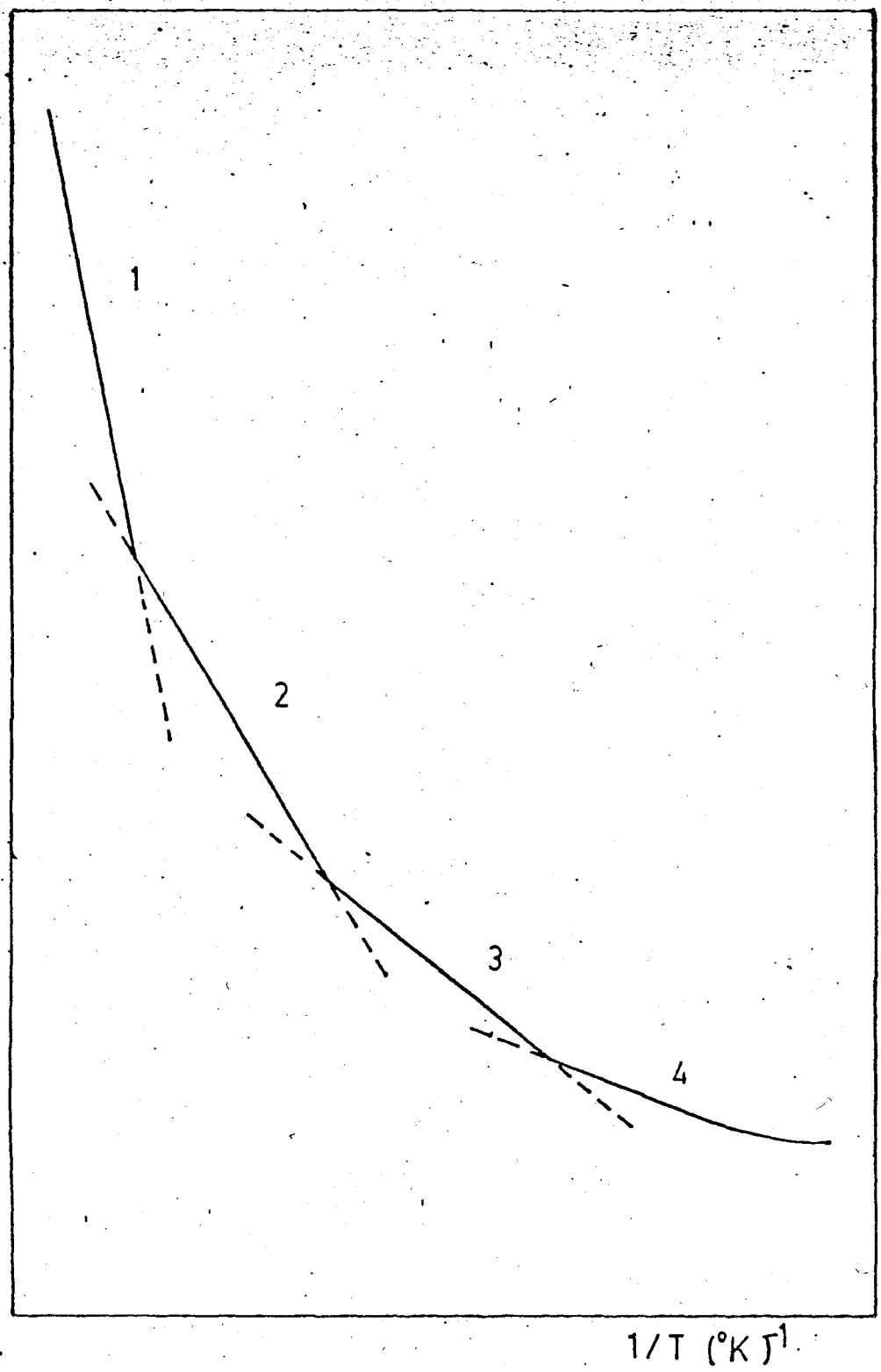


FIGURE 1.2

Temperature Dependence of the DC Conductivity

Activation Energies: 1- Band to Band Conduction

2- Band Tail Conduction

3- Conduction Due to Hopping to the Neighbour

4- Conduction Due to the Variable Range Hopping.

In the temperature range where this equation is valid, $\ln\sigma$ versus $T^{-1/4}$ graph is linear. From the slope of this graph one can obtain $N(E_f)$ by using a proper value of $\alpha$.

A general graph of temperature dependence of the DC conductivity is shown in Figure 1.2.

### 1.2.2 AC Conductivity

As explained in the previous section there are three mechanisms of charge transport that can contribute to a direct current in amorphous semiconductors. They can all contribute to the AC conductivity as follows.

1. Transport by carriers excited into the extended states near $E_c$ or $E_v$. For this, it is expected that the frequency dependent conductivity $\sigma(\omega)$ is given by a formula of

$$\sigma(\omega) = \frac{\sigma(0)}{1-\omega^2\tau^2} \qquad 1.6$$

where $\tau$ is the relaxation time being of the order of $\sim 10^{-15}$ sec A decrease in $\sigma(\omega)$ is not expected until a frequency $\sim 10^{15}$ Hz is reached. In any case, however, this formula is hardly applicable for such small values of $\tau$. It is sufficient to state here that in the electrical range of frequencies (up to say, $10^7$ Hz) no frequency dependence of the conductivity associated with carriers in extended states is expected.

2. Transport by carriers excited into the localized states at the edges of the valence or conduction band:

No complete theoretical treatments of $\sigma(\omega)$ for hopping under this condition are known, but we might expect a similar dependence on frequency to that derived under degenerate conditions (see 3 below), and thus as $\omega \ln^4(\nu_{ph}/\omega)$ This varies approximatel as $\omega^s$, where $s<1$ when $\omega < \nu_{ph}$. In order to estimate the frequency at which such an increase is expected, a comparison with the magnitude of the DC hopping conduction would be required. The temperature dependence of this component of the AC conductivity should be the same as that of the carrier concentration at the band edge, so that for the conduction band it should increase as $\exp -(E_A - E_f)/kT$.

3. Hopping transport by electrons with energies near the Fermi level, provided $N(E_f)$ is finite.

There have been several theoretical treatments of $\sigma(\omega)$ for this mode of conduction(8,10,11,12). $\sigma(\omega)$ should increase with frequency in a manner similar to that for process (2). However, the exponential dependence on the temperature will be absent, and $\sigma(\omega)$ should be proportional to T if kT is small compared with the energy range over which $N(E_f)$ may be taken as constant.

Using the formula given by Austin and Mott(1969)(1)

$$\sigma(\omega) = \frac{1}{3}\pi e^2 kT\left[N(E_f)\right]^2 \alpha^{-5}\omega\left[\ln(\nu_{ph}/\omega)\right]^4 \qquad 1.7$$

where hopping is assumed to be between independent pairs of centres, i.e multiple hopping can be neglected, and also that there is no correlation between the hop energy and the hop distance.

The frequency dependence predicted by equation 1.7 can be written as $\sigma(\omega) = A\omega^s$ , where s is a weak function of frequency if $\omega \ll \nu_{ph}$ :

Equation 1.7 is rewritten as,

$$\sigma(\omega) = A\omega\left[\ln(\nu_{ph}/\omega)\right]^4$$

taking the logarithm of both sides,

$$\ln\sigma(\omega) = \ln A + \ln\left[\omega\ln^4(\nu_{ph}/\omega)\right] \qquad 1.8$$

The slope s is given by,

$$s = \frac{d\left[\ln\left[\omega\ln^4(\nu_{ph}/\omega)\right]\right]}{d(\ln\omega)}$$

$$s = 1 - \frac{4}{\ln(\nu_{ph}/\omega)} \qquad 1.9$$

rewriting the equation 1.8 in the form,

$$\ln\sigma(\omega) = \ln A + s\ln\omega$$

taking the inverse logarithm of both sides,

$$\sigma(\omega) = A\omega^s$$

The plot of $\ln\sigma(\omega)$ versus $\ln\omega$ is therefore approximately linear with slope s given by Equation 1.9.

At a particular frequency, for instance $\omega = 10^4\ s^{-1}$, s varies from 0.4 to 0.8 for $\nu_{ph}$ in the range $10^7$ - $10^{13}$ Hz and values of s outside this range are therefore unlikely.

The Austin-Mott formula yields $\sigma(\omega) = 0$ at $\omega = 0$. Other treatments of AC hopping conduction include the DC limit (11,12). It will be sufficient here to note that the DC conductivity due to hopping is finite (if $T \neq 0$) and a smooth transition to a frequency - independent conductivity is expected at sufficiently low frequencies. A condition for $\sigma(\omega)$ to exceed $\sigma(0)$ is that the AC hopping length should be less than the DC hopping length (1). For variable range hopping, the latter is given by equation,

$$r_o = \frac{3}{4}\left[3/2\pi\alpha N(E_f)kT\right]^{1/4} \qquad 1.10$$

and the AC hopping length,

$$r_\omega = \frac{1}{2\alpha}\ln(\nu_{ph}/\omega) \qquad 1.11$$

The frequency dependence of the conductivity expected for the three conduction mechanisms outlined above are schematically illustrated in Figure 1.3.

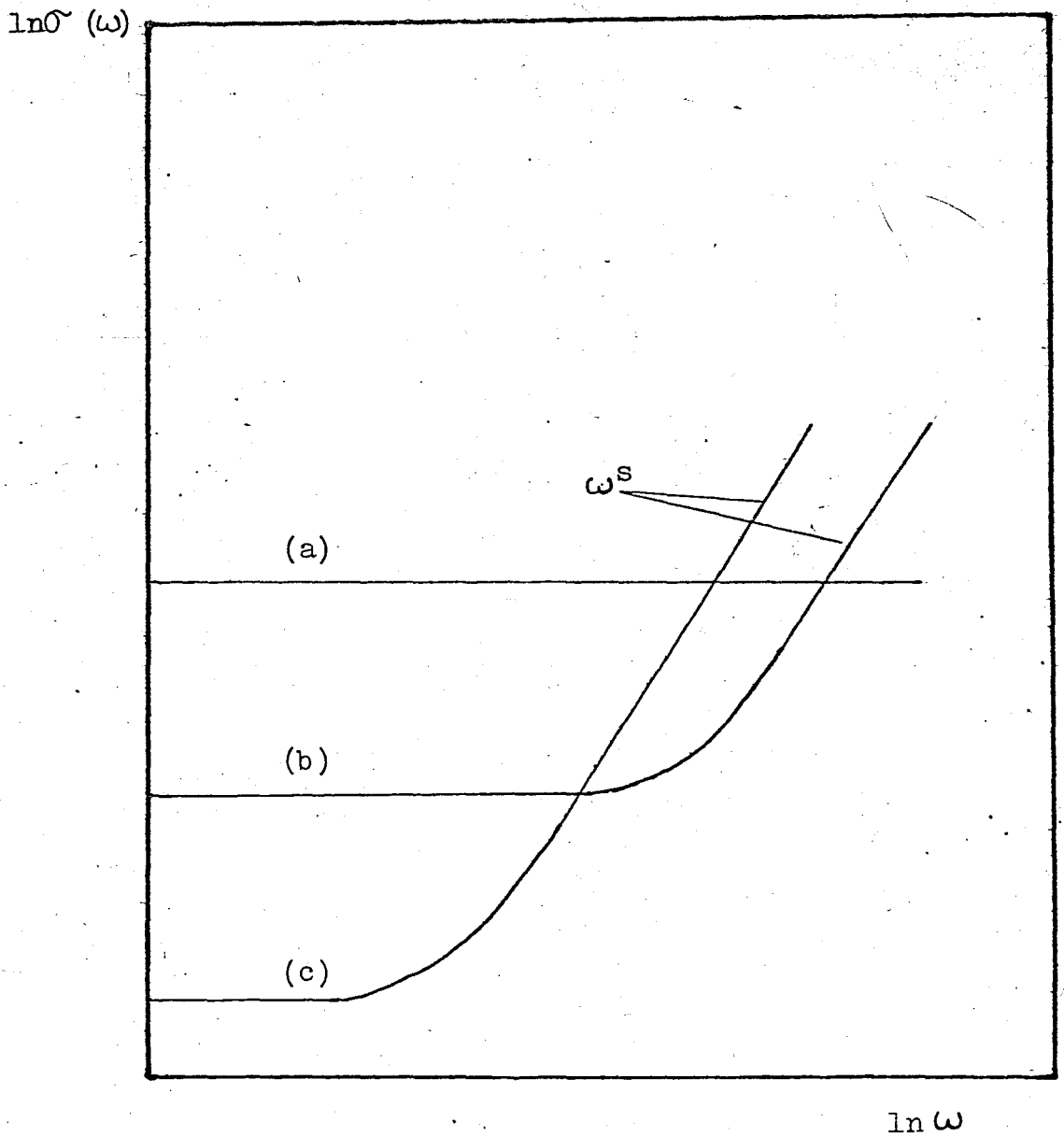


FIGURE 1.3

Schematic Illustration of the Frequency Dependence of Conductivity for the Three Modes of Conduction

a) Extended State Conduction b) Band Tail Conduction

c) Hopping Conduction around the Fermi Level.

# II. EXPERIMENTAL TECHNIQUES

## 2.1 PREPARATION OF THE FILMS

The amorphous silicon films and metal electrodes are evaporated in a coplanar geometry on microscope slides, by 2.5 x 4.5 cm in length, produced by Fisher Scientific Co. The masks used in the evaporation process for silicon films and the metal electrodes are shown in Figure 2.1. The evaporation masks are made of aluminium metal plate of 0.55 mm thickness. Wires of 0.22 mm, 0.30 mm and 0.37 mm diameters are placed in the rectangular space (1.5 x 2.5 cm) of the metal electrode masks to produce a coplanar geometry.

Microscope slides are first cut to the desired dimensions and then cleaned with alconox detergent in an ultrasonic vibrator. They are then rinsed with distilled water, methanol and aceton.

The vacuum system is VARIAN VT - 422 type. The system is pumped down to $10^{-3}$ torr pressure with a cryopump. In order to achieve a lower pressure ion pumps are used. The pumping time of the cryopump is approximately one hour. Ion pumps operate continuously for 12 hours to drop the base pressure to $10^{-7}$ - $10^{-8}$ torr. The pressure is measured with a thermocouple pressure gage down to $10^{-3}$ torr and below that value with an ion gauge. The glass substrates are placed on a substrate holder, produced by VARIAN, on which three different masks can be prepared at a time.

The evaporation system used consists of an electron-gun and three crucibles produced by VARIAN. The evaporant is a pure polycrystal lump obtained from Matheson Coleman and Bell laboratories. The distance between the evaporant and the glass substrate is 25 cm. To avoid the risk of impurity atoms contaminating the film, the base pressure must be kept as low

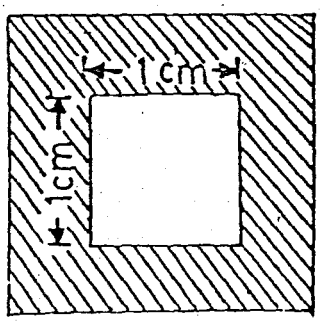


(a)

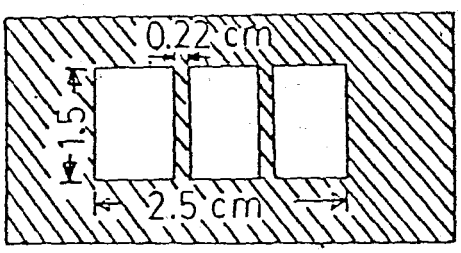


(b)

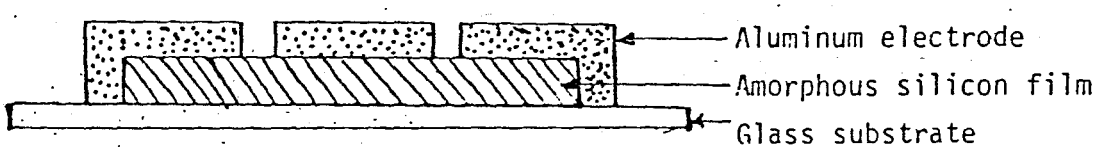


(c)

FIGURE 2.1
Masks Used in the Preparation of Amorphous Silicon Films
(a) Silicon Mask
(b) Electrode Mask Prepared in Coplanar Geometry
(c) Cross-Section of the Prepared Film in Coplanar Geometry

as possible. The base pressure before evaporation is decreased to $10^{-8}$ torr, while during evaporation it is kept constant at $5 - 7 \times 10^{-7}$ torr. This is achieved by circulating liquid nitrogen through a jacket around the vacuum chember. The film thicknessess are between 0.30$\mu$m and 0.60$\mu$m. The evaporation of the silicon films takes between two to four hours. After the deposition of the silicon films, the vacuum system is allowed to cool in order to prevent the formation of an oxide layer on the film. Then the system is opened and prepared for the evaporation of aluminium electrodes. The thickness of the electrodes is around 1$\mu$m. and they are evaporated in 1-2 min. The thickness of the evaporated films is measured with an $A^{o}$ scope interformeter produced by VARIAN. A quartz crystal digital thickness monitor produced by SLOAN is used to adjust the evaporation rate. However, it could not be used to determine the thickness of the films since the density of the films is not known.

## 2.2 EXPERIMENTAL SET-UP

### 2.2.1 Thermostatic Chamber

During the AC and DC measurements the samples are kept in a thermostatic chamber. The schematic diagram of the thermostatic chamber is shown in Figure 2.2.

The temperature of the sample holder can be lowered to - 190$^{o}$C by filling the reservoir under the sample holder with liquid nitrogen and with the aid of a heater can be raised up to 600$^{o}$C. An electronic control unit is used to keep the temperature constant within 0.50$^{o}$C deviations. At lower temperatures, to avoid the condensation of vapor of water on the sample and to prevent heat transfer between the thermostatic chamber and its environment, the air inside the thermostatic room is continuously pumped out.

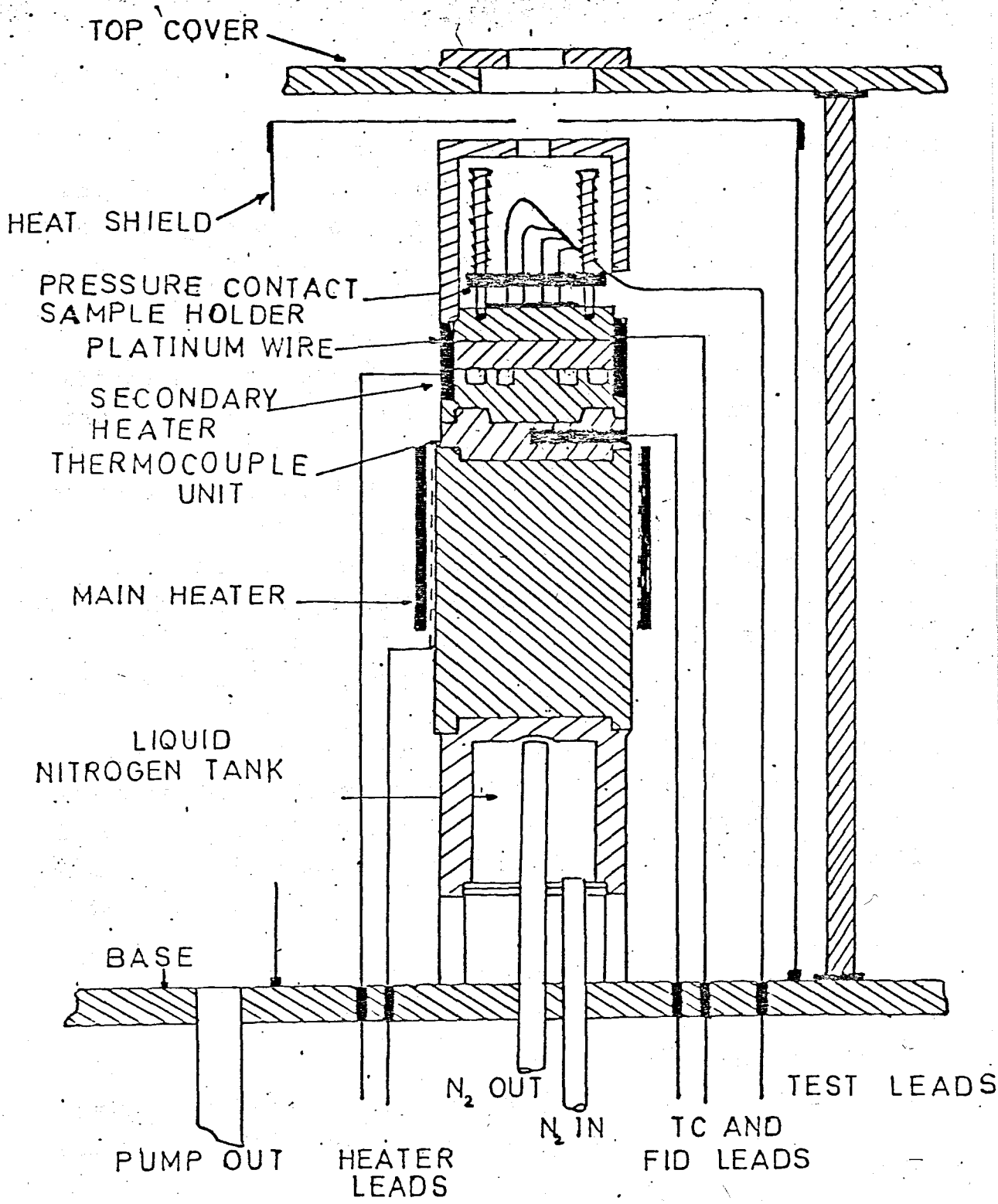


FIGURE 2.2
Schematic Diagram of the Environmental Chamber

### 2.2.2 DC Measurements

DC measurements include I-V measurements at room temperature and I-T measurements at constant electric field. The block diagram of the apparatus used in these measurements is given in Figure 2.3.

In order to take the I-V measurements the applied voltage is changed manually in 5 volt steps to achieve electric fields of $10^2$ V/cm to $10^3$ V/cm. The current for each setting is recorded after it stabilizes in order to avoid any capacitive effect. Applied voltage is measured with a digital voltmeter connected across the DC power supply so that the ammeter indicates the current that passes through the sample. Since the internal resistance of the voltmeter is comparable with the sample resistivity the total current is much greater than that flowing through the sample.

The major difficulty encountered during the measurements is the environmental noise which increases with the increase in sample resistivity as the temperature is lowered. Thus, every connection has to be shielded in order to avoid this problem.

### 2.2.3 AC Measurements

AC measurements include frequency-dependent conductivity measurements under constant temperature and I-T measurements at several different frequencies.

AC measurements were made in the frequency range of 100Hz - 1MHz and in the temperature range of 77 - 300°K. A Hewlett - Packard 4192A impedance analyzer was used for frequency dependent conductivity measurements.

The AC signal level was kept at a level of 0.7V - 1.1V, in order to prevent the effect of the field on the conductivity of the sample.

Again, the major difficulty encountered with the high resistivity samples is environmental noise, and to overcome this problem every connection was shielded. We therefore used 50Ω coaxial cables.

In order to make sure that there was no residual conductance, open circuit conductance measurements were made throughout the entire frequency range (up to 1 MHz) employed in the sample measurements and 0.000$\mu$S were obtained.

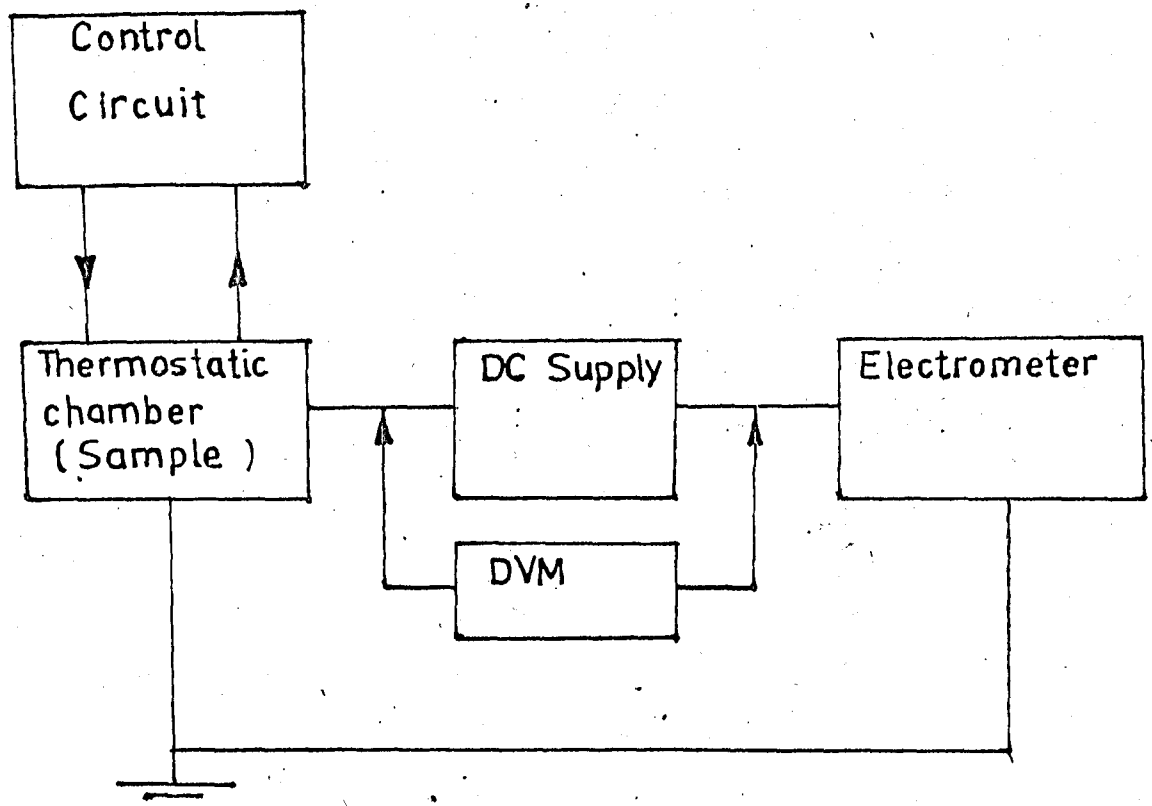


FIGURE 2.3

The Block Diagram of the Apparatus Used in DC Measurements

# III. EXPERIMENTAL RESULTS

## 3.1 DC MEASUREMENTS

The I-V characteristic of the films are obtained using the set-up in Figure 2.3 at room temperature and under a DC voltage of 5V - 50V corresponding to electric fields of $10^2$ - $10^3$ V/cm. Philips PE 1520 was used as the DC power supply. In order to measure the currents around $10^{-8}$ - $10^{-14}$ amperes a Cary 401 vibrating Reed electrometer was used and for larger values of current at higher temperatures a Keithley Digital Electrometer was used.

DC measurements are done for two purposes,

i) I-V measurements at room temperature are performed to verify whether the contact between the metal electrode and the amorphous semiconductor is ohmic or not and also to have a first-hand idea of the effects of the preparation conditions on the structure of the film.

ii) Temperature dependent conductivity measurement were performed to determine the conductivity mechanism and the density of localized states near the Fermi level.

### 3.1.1 I-V Measurements at Room Temperature

The I-V measurements of the samples show that the I-V graph is symmetric with respect to the polarity of the voltage applied, implying that the aluminium electrodes form an ohmic contact with the amorphous semiconductor film which implies that there is no contact barrier and the conductivity of the surface states is negligible compared to the conductivity of bulk states.

As seen from Figure 3.1 there is an ohmic region, which goes up to $10^3$ V/cm in most samples. The ohmic behaviour disappears after this region and the current increases exponentially at higher electric fields. According to the Poole-Frenkel theory (6) this may be due to the presence of high electric field effects on the coulombic potential barrier. The potential barrier can be lowered such that the thermal energy, which is not enough to release the trapped electron in the absence of the field, becomes sufficient to emit the electron in the presence of the electric field E. In this case the free electron with the help of the electric field, will jump to the conduction band where its contribution to the conduction is considerable. The current will therefore be of the form,

$$I = A(T)\, E^{a} \exp\left(\frac{e\beta E^{1/2}}{kT}\right) \qquad 3.1$$

where $\beta$ is the Poole-Frenkel constant, e is the electron charge, a is an exponent of the order of 1 or 2 and A(T) is a function of temperature. Since the dominant field dependence is through the exponential term, the $E^a$ factor has a relatively weak contribution.

### 3.1.2 Temperature Dependence

Current versus temperature (I-T) measurements were performed between 77°K to 430°K at 10°C or 20°C temperature intervals under a constant electric field. The results obtained for two samples are shown in Figures 3.5 and 3.6 (labelled 0 Hz curves).

In the higher temperature range, the conductivity mechanism involved is band to band conduction.

The activation energies obtained from the slopes of $\ln\sigma$ versus $T^{-1}$ graphs above 400°K are around 0.5 - 0.6 eV, which are nearly the half of the energy gap according to Equation 1.1 assuming that $E_f$ is in the middle of the gap. These values show that the mobility gap of amorphous silicon lies around 1.1 eV. These values agree with the values obtained by other researchers (13). Therefore at temperatures above 400°K the conduction mechanism is a band to band conduction.

In the temperature range between 400°K and 289°K a different conduction mechanism exist since the curve is not linear any more. In this temperature range, electrons hop to tail states closer to the conduction band. The activation energies for this range are 0.35 eV and 0.44 eV for two samples as shown in the figures.

The activation energies obtained from the slopes of $\ln\sigma$ versus $T^{-1}$ graphs between 289°K and 200°K are between 0.27 eV and 0.18 eV. This shows us that the conduction mechanism involved is preferrably hopping conduction between the nearest neighbours (14).

At variable range hopping region the activation energies are around 0.10 eV.

## 3.2 AC MEASUREMENT

AC conductivity measurements were performed with a Hewlett-Packard 4192A LF impedance analyzer, in the frequency range 100 Hz - 1 MHz and in the temperature range 77°K-300°K.

AC conductivity was measured as a function of frequency at a constant temperature and the measurements were repeated at different temperatures. $\sigma(\omega)$ versus $T^{-1}$ graphs at constant frequency were constructed using this data.

Frequency dependent measurements at variable range hopping region are used to calculate the density of states at the Fermi level. The DC data (i.e DC conductivity versus temperature measurements) were used to determine the temperature range where variable range hopping is the dominant conduction mechanism, and the above mentioned AC measurements were taken at a corresponding temperature. Temperature dependent AC measurements were used in comparison with temperature dependent DC measurements (Fig. 3.5 - 3.6)

### 3.2.1 Frequency Dependent Mesurements

Conductance versus frequency measurements were taken in the frequency range 100 Hz - 1 MHz. The results obtained for the samples are shown in Figures 3.9 and 3.10. Similar results are found by other workers (8,11,12,15).

For sample 17.11.85 -I, measurements taken at 162$^{o}$K and 77$^{o}$K (Fig. 3.9) correspond to variable range hopping conduction since there is no frequency independent region in these curves. If one takes a look at the I-$T^{-1}$ curve of the same sample (Fig. 3.5) it can be seen that there is a kink around 162$^{o}$K indicating a change in the dominant conduction mechanism which is interpreted as a change from variable range hopping to nearest neighbour hopping.

The same situation is also observed for the sample 27.III.86 -I. In this case, one can easily see that on the I-$T^{-1}$ curve of the same sample, a different conduction mechanism occurs after 180$^{o}$K.

In both samples, in the variable range hopping region, the slope of the frequency versus AC conductivity curves, s has the same value of 0.87 in agreement with the results of other researchers. Their results vary between 0.5 - 1.0, the most common results being 0.8 - 0.9 (8,11,15,16,17).

In both samples, frequency dependent conductivity measurements taken at higher temperatures, each shows two distinct regions : first, a frequency independent region which becomes larger with increasing temperature. At room temperature the region ends around $10^2 - 10^3$ Hz. Second, a frequency dependent and weakly temperature dependent region, in accordance with the AC conductivity theory mentioned in 1. 2. 2 and schematically shown in Figure 1. 3.

### 3. 2. 2 Temperature Dependence of AC Conductivity

In Figures 3. 5 and 3. 6 temperature dependence of AC conductivity is shown. As is observed in both graphs, the higher the frequency the weaker the temperature dependence. Both the DC curves (labelled OHz) and the AC curves are in agreement with the respective theories explained in the previous chapter.

The DC curve is completely temperature dependent whereas in the AC curves the temperature dependence decreases as the frequency increases. At higher temperatures all the curves approach the DC curve (Fig. 3. 5 - 3. 6).

## 3. 3 MEASUREMENT OF DENSITY OF STATES

The density of states at the Fermi level can be determined from the DC measurements using Mott 's formula (Equation 1. 4 and 1. 5) and also from the AC measurements using Austin-Mott 's formula (Equation 1. 7).

For the former case, in the low temperature range below 200$^{o}$K and at constant electric field of $10^2 - 10^3$V/cm, the conductivity versus $T^{-1/4}$ graphs of the two samples are plotted. These graphs are shown in Figures 3. 7 and 3. 8. In this temperature range there is a linear relation in accordance

with the variable range hopping conductivity proposed by Mott. Equation 1.4 can be rewritten as,

$$\ln\sigma = \ln\sigma_o - (T_o/T)^{1/4}$$

Therefore, the density of localized states around the Fermi level $N(E_f)$ can be calculated from the slope of the $\ln\sigma$ versus $T^{-1/4}$ graph. By taking $\alpha^{-1} = 10\ A^o$ as proposed by Mott (1) for evaporated Si films, the $N(E_f)$ values were calculated for the two samples (Eq. 1.5). The results are as follows;

| Sample | $N(E_f)$ $(cm^3 - eV)^{-1}$ |
|---|---|
| 17.11.85-I | $7.57 \times 10^{17}$ |
| 27.III.86-I | $6.65 \times 10^{17}$ |

The Austin-Mott formula (Eq. 1.7) was used to calculate $N(E_f)$, from the AC data. If this model is valid, $\log\sigma$ should have a linear dependence on $\log\omega$ in the variable range hopping region. As mentioned earlier, low temperature curves, in Figures 3.9 and 3.10, show this behaviour and thus values taken from these curves were used in the calculation of $N(E_f)$. Taking $T = 77^oK$, $f = 10^4$ Hz, $\nu_{ph} = 10^{13}$ Hz, and the corresponding AC conductivity value, $N(E_f)$ was calculated. The results are as follows,

| Sample | $N(E_f)$ $(cm^3 - eV)^{-1}$ |
|---|---|
| 17.11.85-I | $4.74 \times 10^{19}$ |
| 27.III.86-I | $2.74 \times 10^{19}$ |

The $N(E_f)$ values deduced from AC measurements are higher than those obtained from DC measurements.

This situation has been also observed by other researchers (1,8).

The calculated $N(E_f)$ values (from variable range hopping DC measurements and from AC conductivity measurements) are plotted as a function of the DC conductivity in Figure 3.11. As predicted by both AC and DC theories $N(E_f)$ must increase with increasing conductivity at variable range hopping region. This systematic variation is more clearly evident from AC results.

The $N(E_f)$ values calculated by some workers using different techniques for evaporated amorphous silicon films are as follows,

i) K.P. Chick and K.C.Koon(1986) calculated $N(E_f) = 6 \times 10^{19}$ $(cm^3 - eV)^{-1}$ using direct measurement of electron spin density (14).

ii) N.Balkan, P.N.Butcher, W.R.Hogg, A.R.Long and S.Summerfield(1985) measured $T_o = 2.66 \times 10^7$ $^oK$ (18) giving $N(E_f) = 7.86 \times 10^{18}$ $(cm^3 - eV)^{-1}$ (According to the Equation 1.5).

These results imply that the $N(E_f)$ values calculated from AC data are more realistic.

## 3.4 THE EFFECT OF PREPARATION CONDITIONS

It is well known that electrical and optical properties of amorphous semiconductors depend on the preparation conditions (1, 2, 4).

The resistivity of the amorphous silicon films can be changed by changing the deposition rate. Decreasing the deposition rate increases the resistivity of the films. This is

believed to be due to prevention of the voids occuring during deposition. When the deposition rate is kept low, the atoms find time to arrange themselves before they are covered by other atoms.

Ageing is another effect on the resistivity of the films. This attributed to the saturation of dangling bonds in time.

The annealing effect is more pronounced for the samples deposited at relatively low temperatures. For example, the resistivity of Sample 17.11.85-I was increased by a factor of 100 by annealing at 300°C for two hours (Fig. 3.3 and 3.4), whereas Sample 27.III.86-I was deposited at about 300°C and its resistivity was increased only by a factor of 2 by annealing at 300°C for two hours (Fig. 3.1 and 3.2)

The resistivities of the films are as follows, (at room temperature)

| Sample | Resistivity ($\Omega$.cm) |
|---|---|
| 17.11.85-I | $2 \times 10^6$ |
| 27.III.86-I | $1.13 \times 10^7$ |

The resistivities of the amorphous Si films prepared with the electron gun evaporation method by other researchers are as follows (19, 20, 21),

| Researchers | Resistivity ($\Omega$.cm) |
|---|---|
| Yang, John and Wong | $10^7 - 10^8$ |
| Dey and Fong | $10^5 - 10^6$ |
| Dellaferra, Labusch and Roscher | $10^3 - 10^4$ |

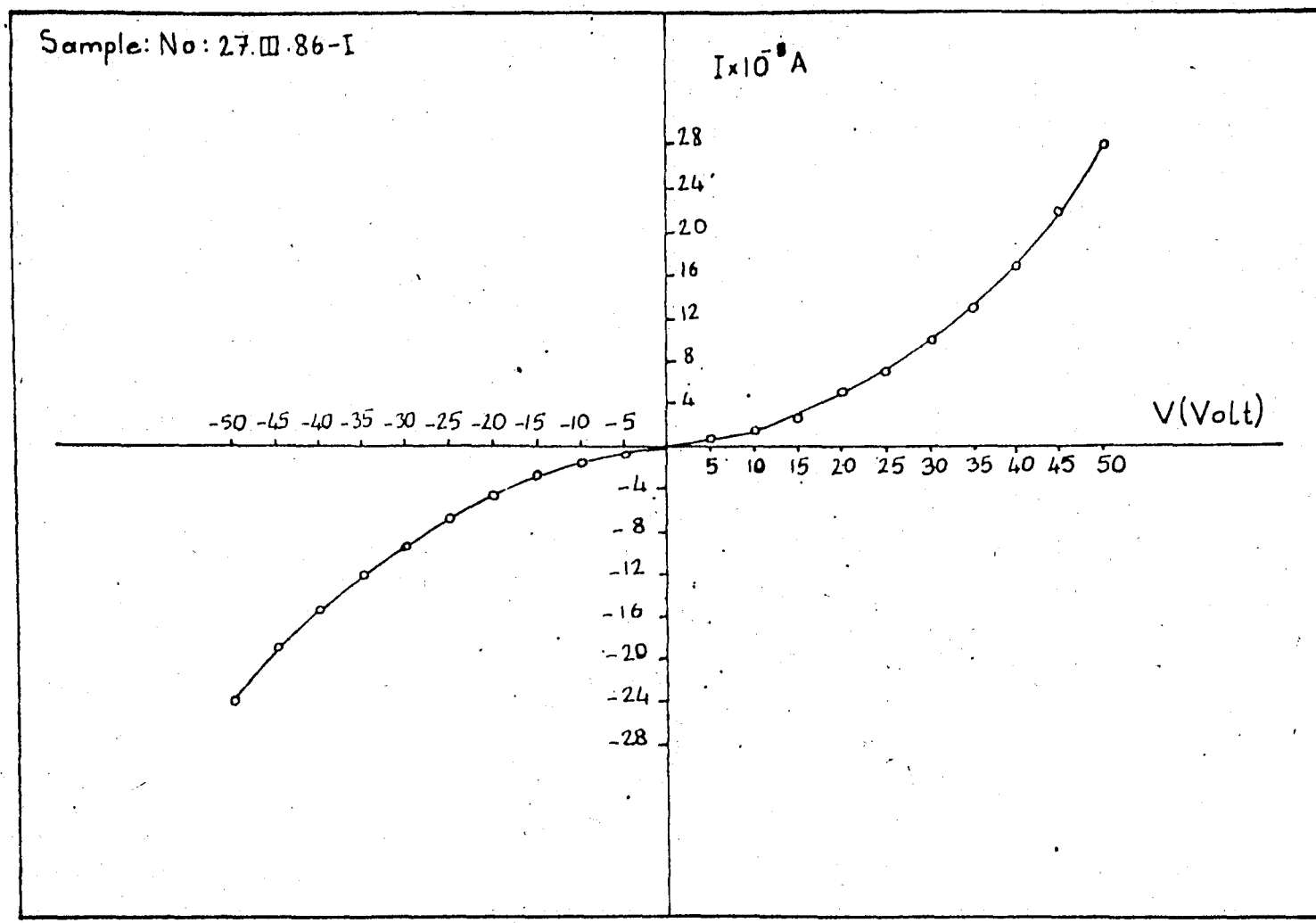


FIGURE 3.1
I-V Curve of a Sample at Room Temperature (Before Annealing)

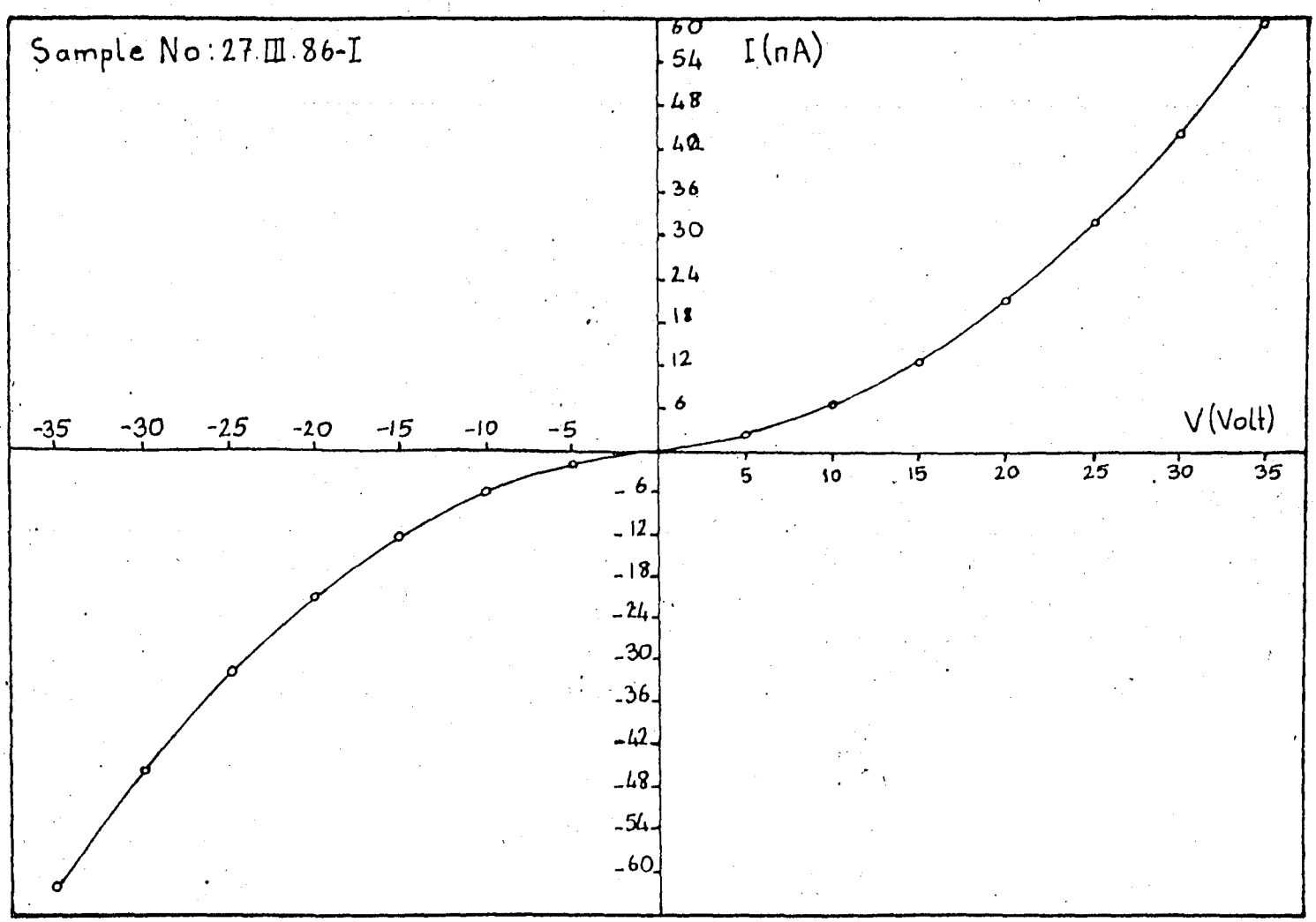


FIGURE 3.2

I-V Curve of a Sample at Room Temperature (After Annealing)

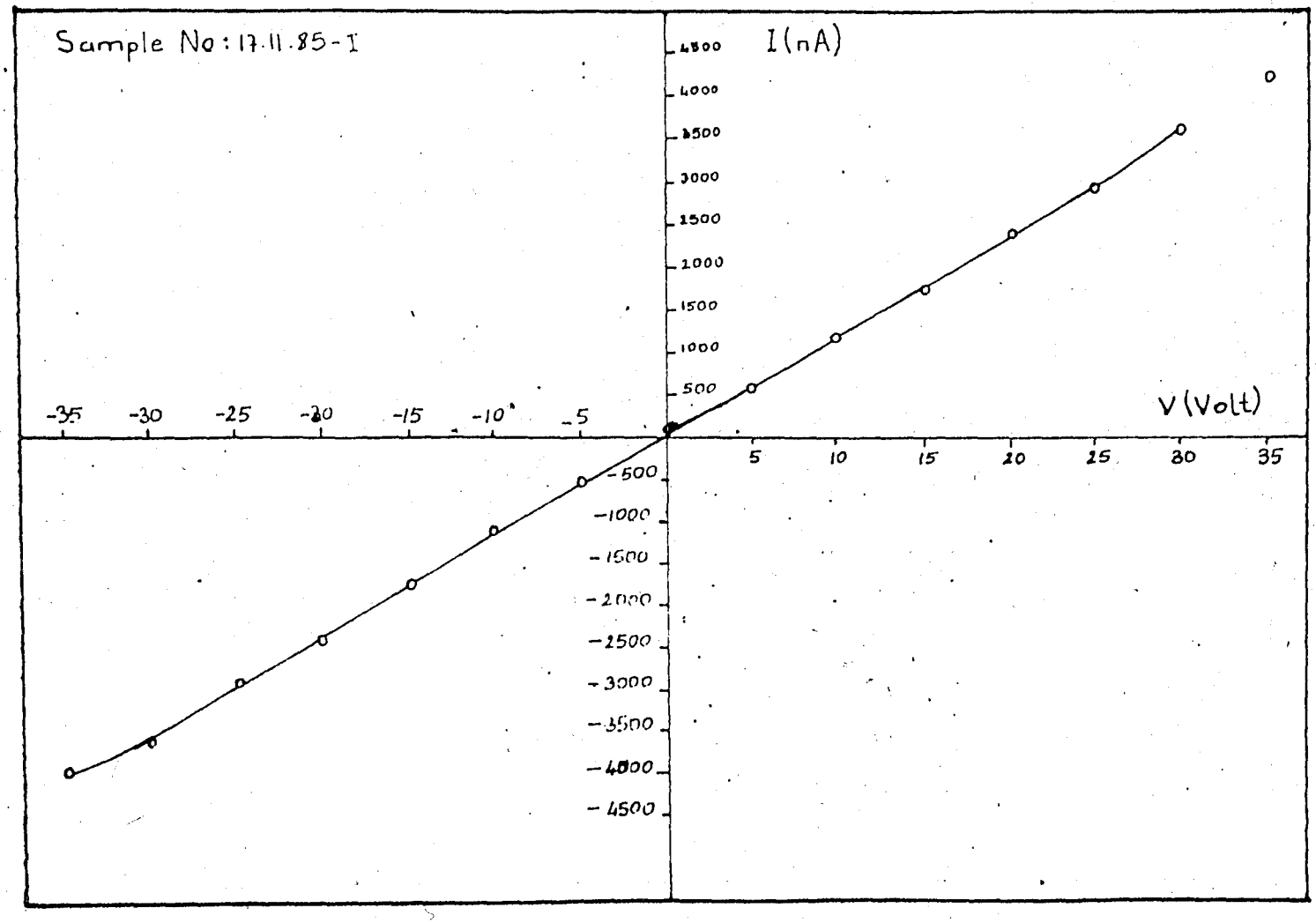


FIGURE 3.3

I-V Curve of a Sample at Room Temperature (Before Annealing)

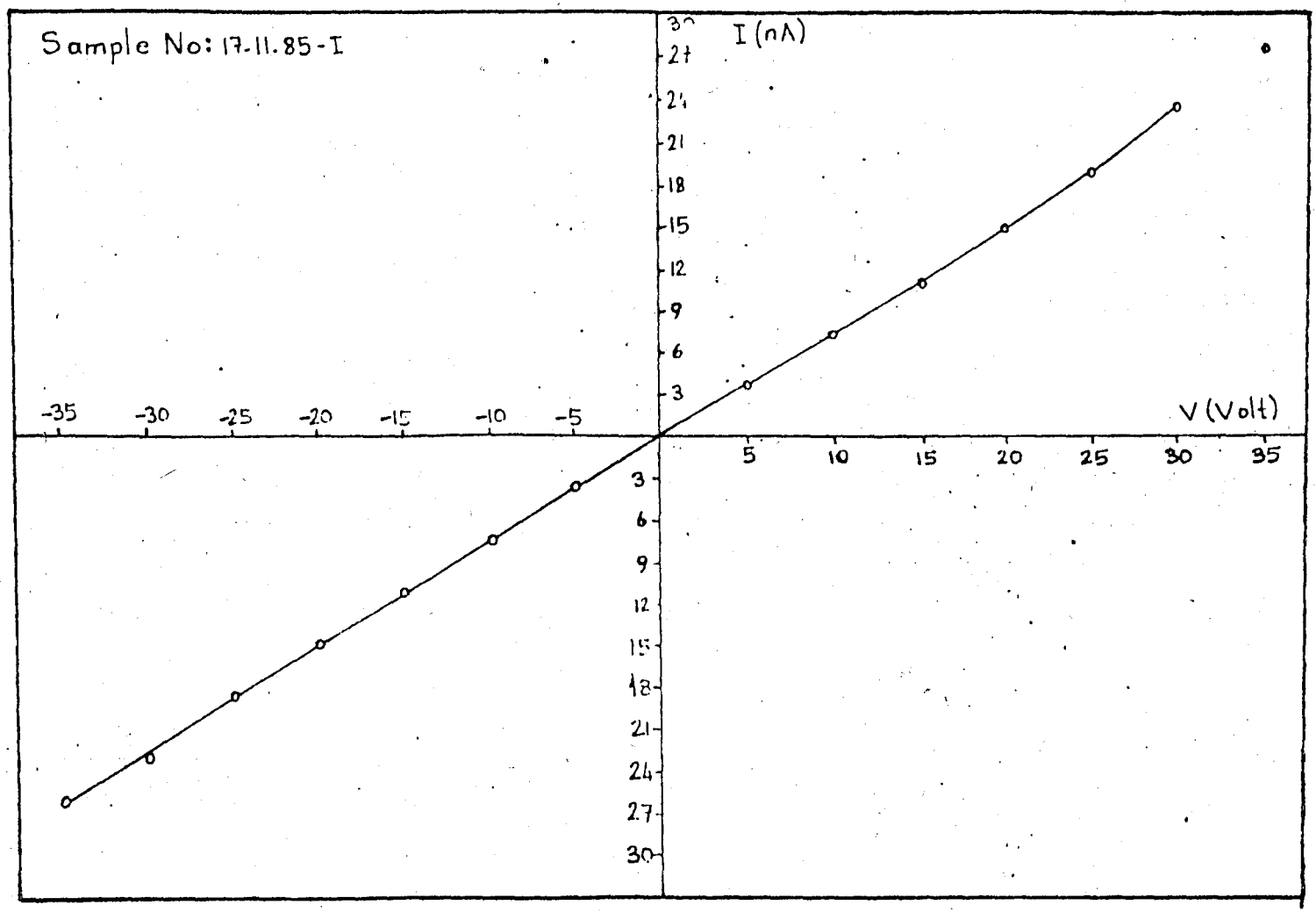


FIGURE 3.4

I-V Curve of a Sample at Room Temperature (After Annealing)

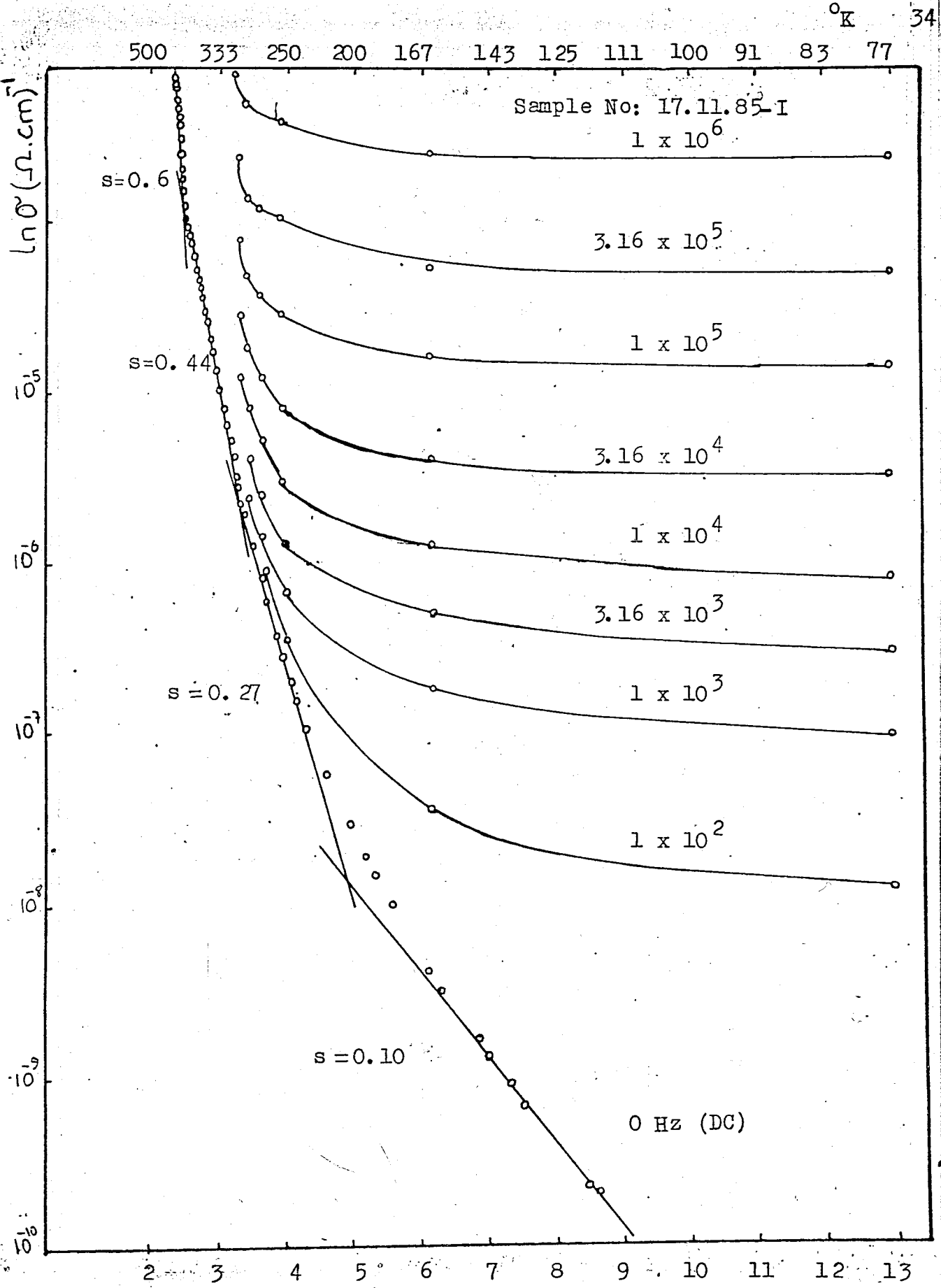


FIGURE 3.5
The Conductivity versus $T^{-1}$ graph of a sample at Several Different Frequencies.

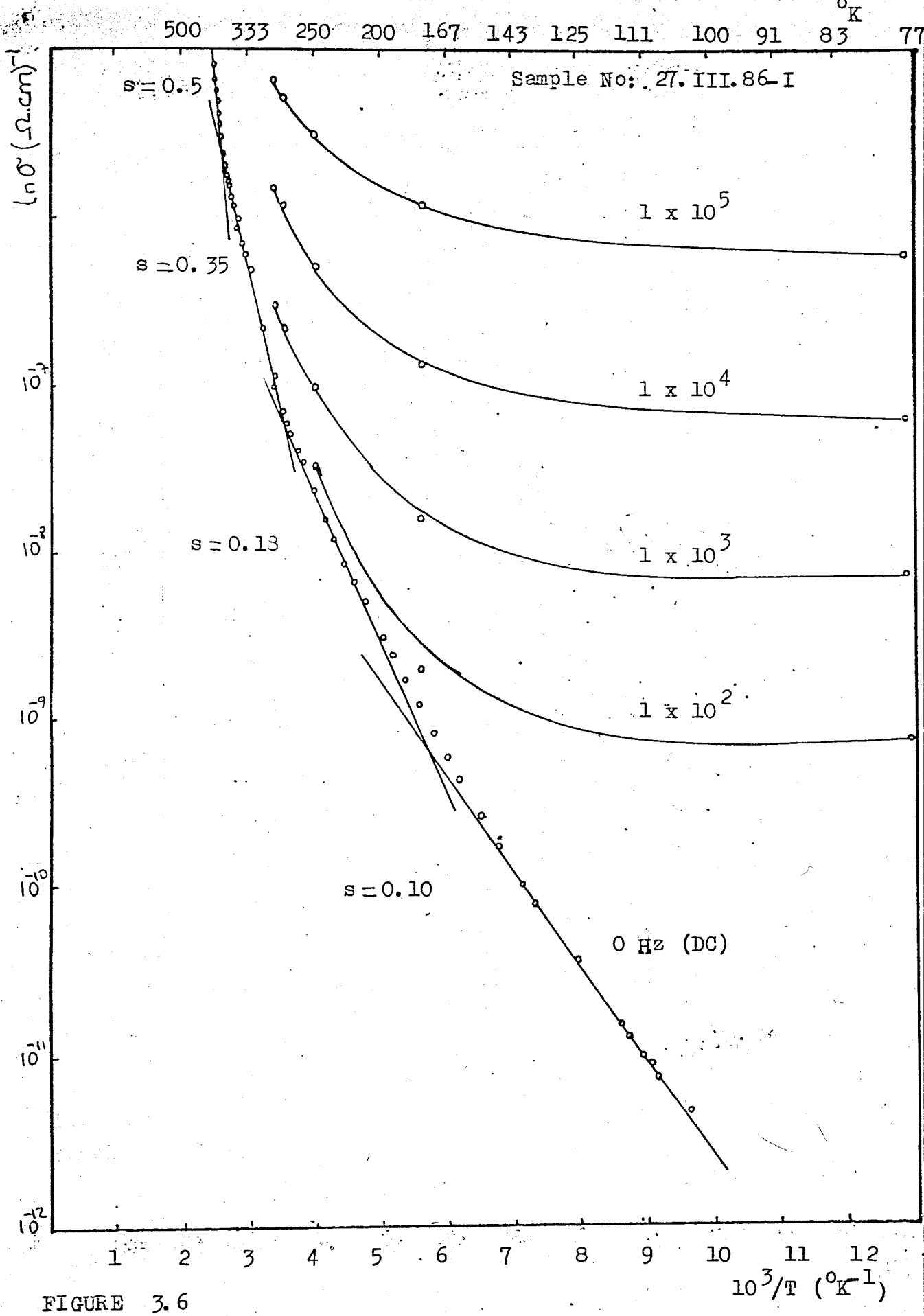


FIGURE 3.6

The Conductivity Versus $T^{-1}$ graph of a Sample at Several Different Frequencies.

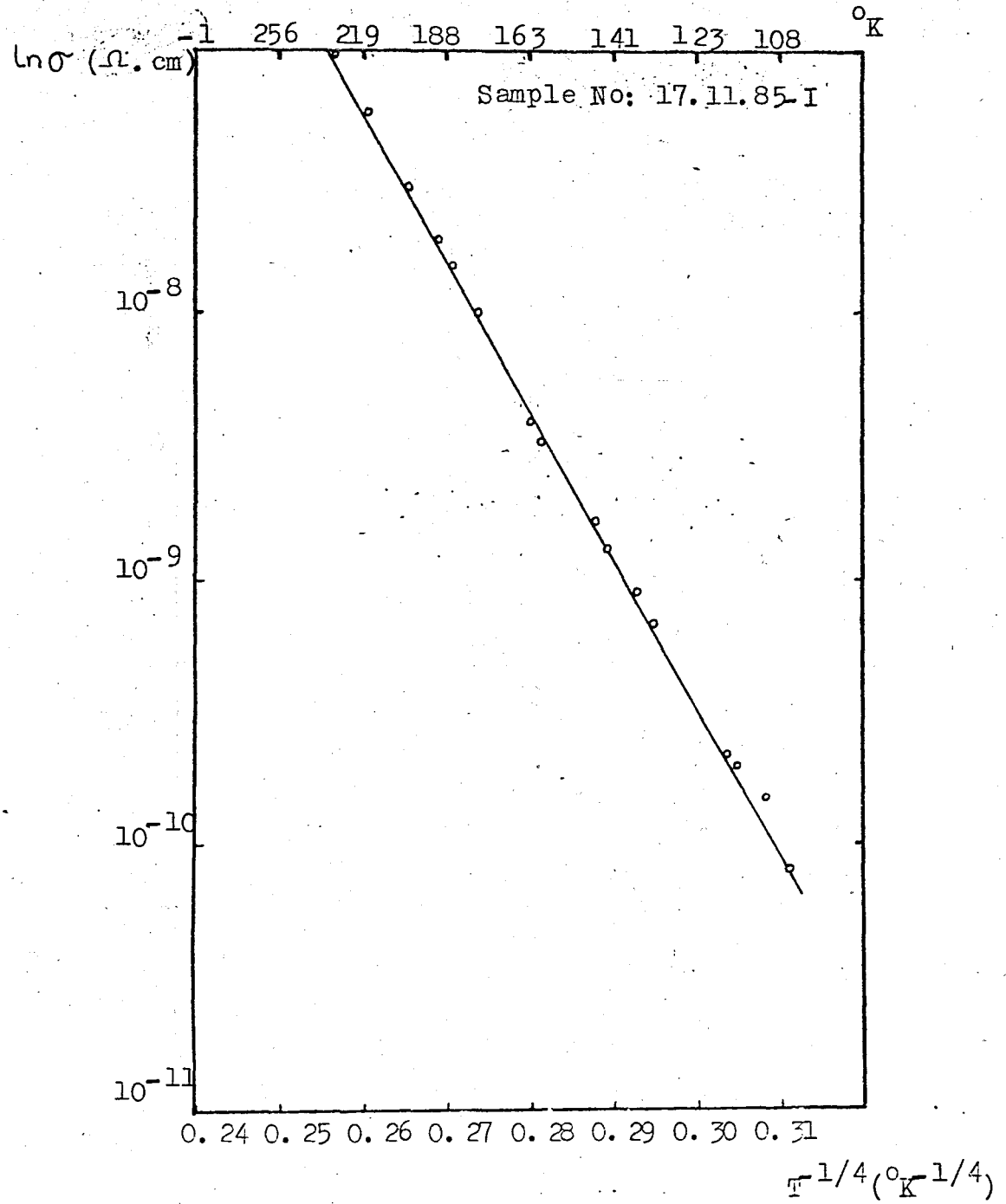


FIGURE 3.7

The Variation of Conductivity as a Function of $T^{-1/4}$ of Sample 17.11.85-I

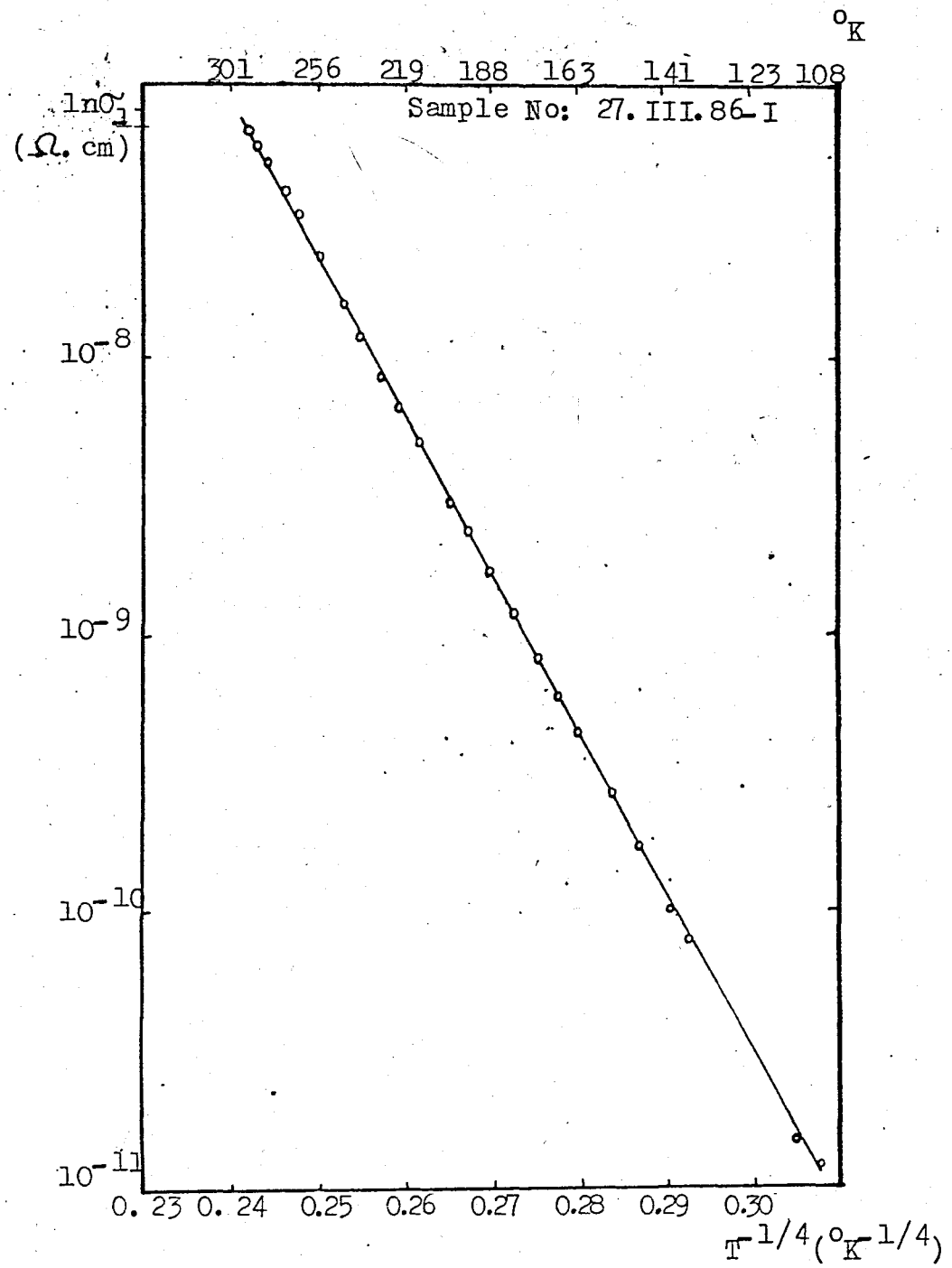


FIGURE 3.8
The variation of Conductivity as a Function of $T^{-1/4}$ of Sample 27.III.86-I

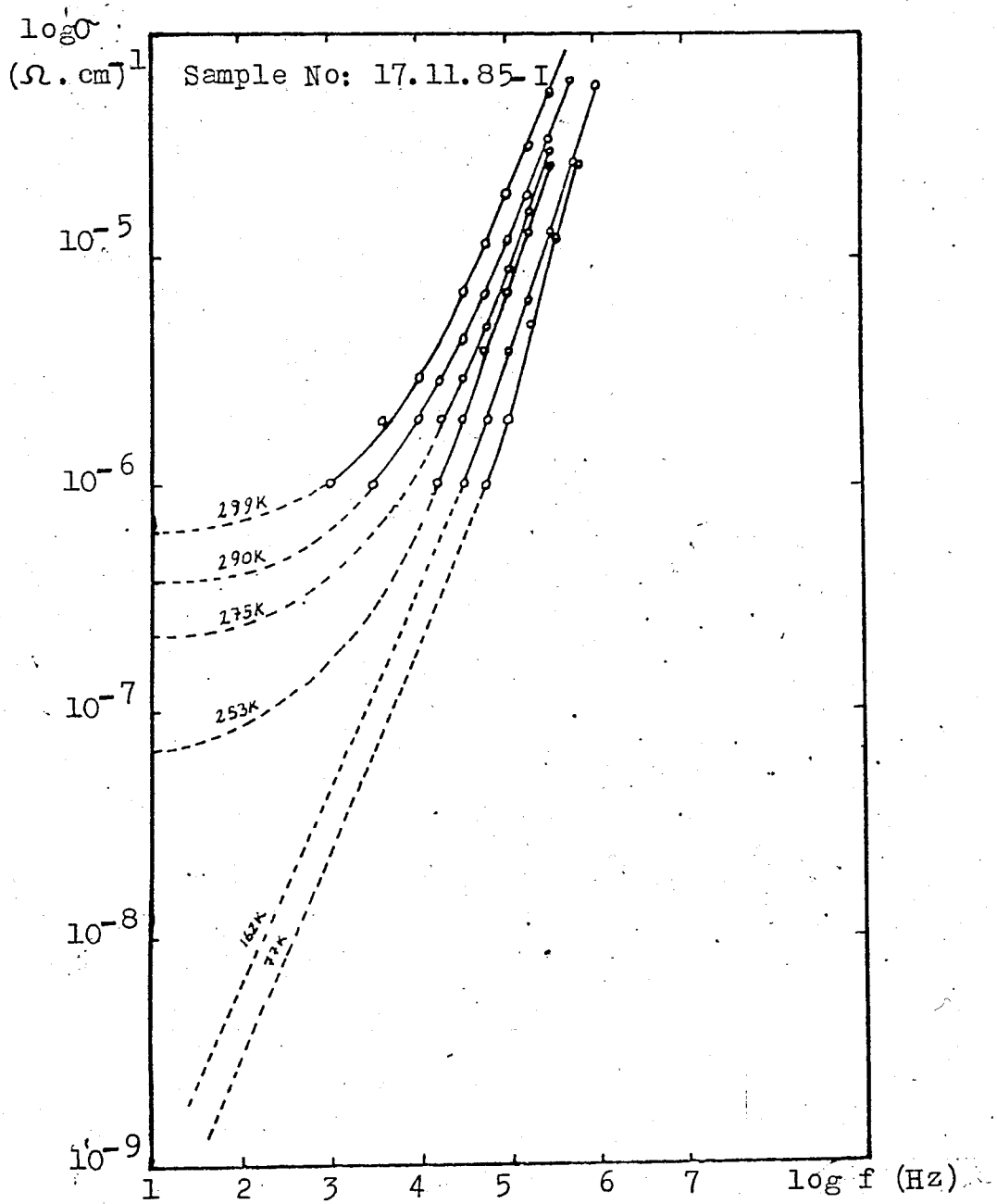


FIGURE 3.9
Frequency Dependence of the Conductivity at the Indicated Temperatures.

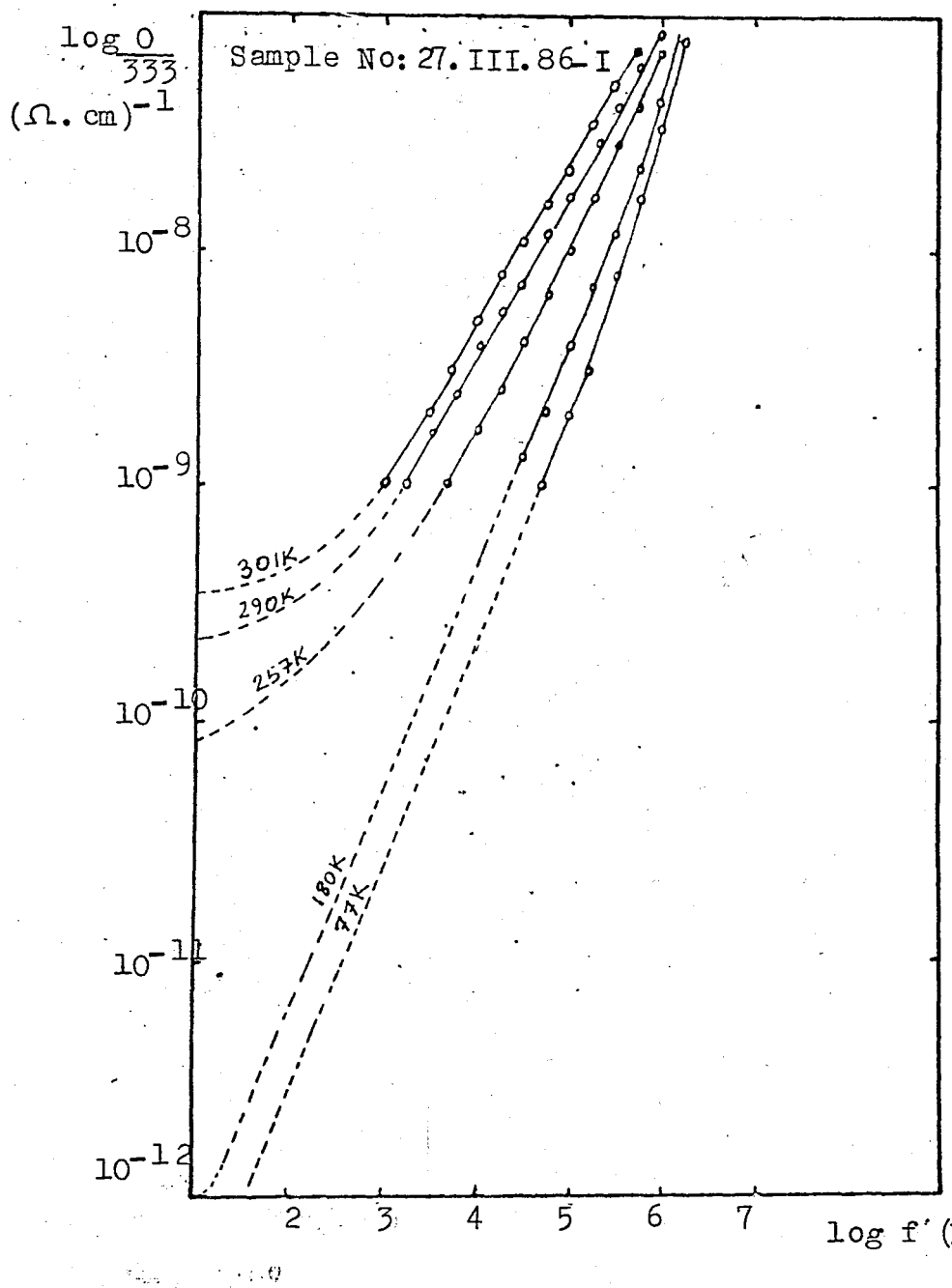


FIGURE 3.10

Frequency Dependence of the Conductivity at the Indicated Temperatures.

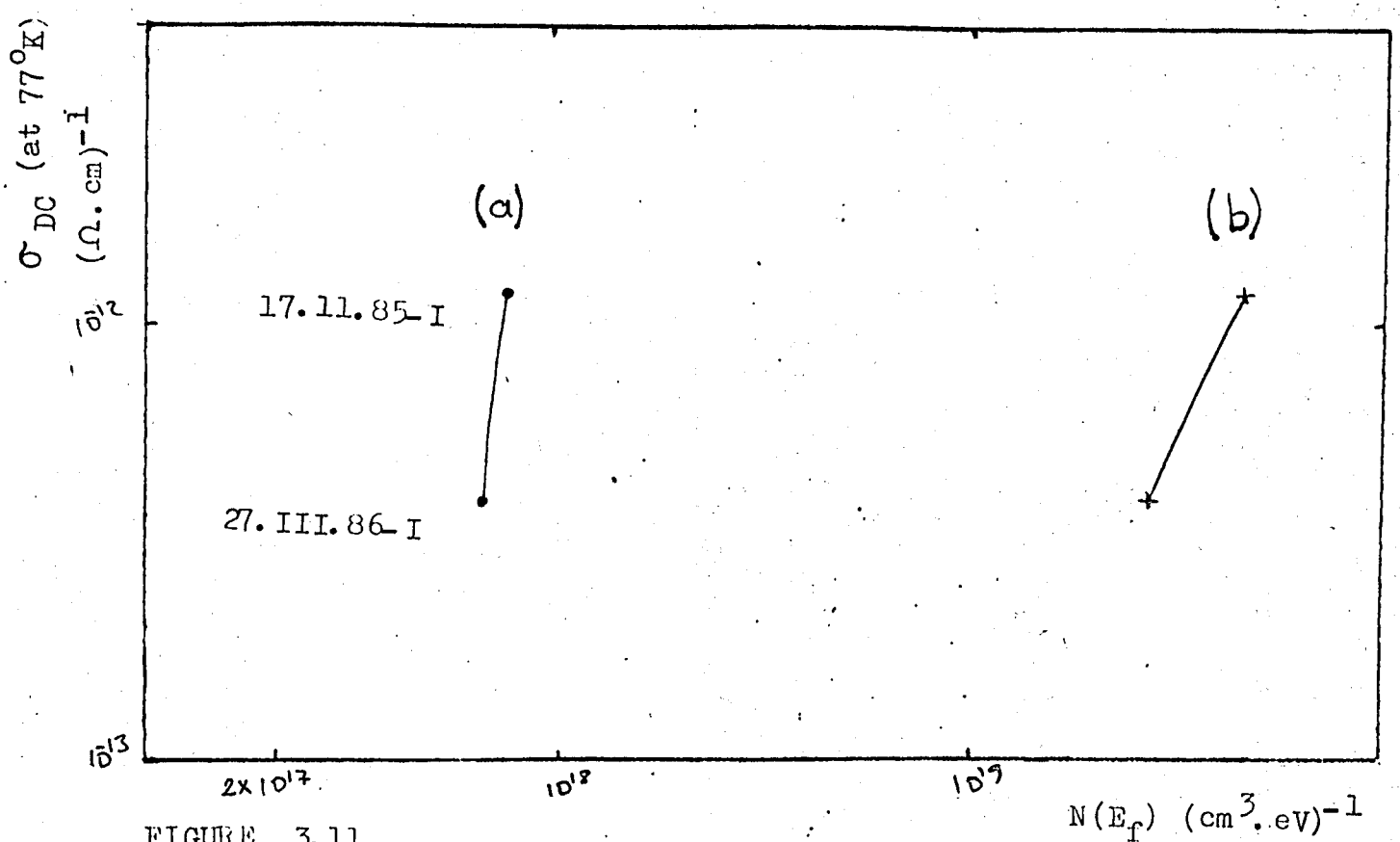


FIGURE 3.11

DC Conduction (at 77°K) Plotted Against the Density of States at the Fermi Level Determined a) From Variable Range Hopping DC Data and b) From AC Conduction Measurements on the Same Samples

# IV. CONCLUSION

In order to investigate such electrical properties of amorphous silicon as the room temperature conductivity, basic transport mechanisms, and activation energies; DC and AC measurements were performed in the temperature range from $77^{\circ}K$ to $400^{\circ}K$. I-V measurements at room temperature show that the contacts are ohmic up to an electric field of $10^3$ V/cm. At high electric fields the I-V curve obeys the Poole-Frenkel law, so that the conductivity increases exponentially.

The DC conductivities of films are around $5 \times 10^{-7}$ and $8.88 \times 10^{-8}$ $(\Omega . cm)^{-1}$ at room temperatur and $3.38 \times 10^{-13}$ and $7.78 \times 10^{-14}$ $(\Omega . cm)^{-1}$ at $77^{\circ}K$.

In the higher temperature range above $400^{\circ}K$ the conduction mechanism is band to band conduction. The activation energies obtained from the slope of $\ln\sigma$ versus $T^{-1}$ graphs above $400^{\circ}K$ are around 0.5 - 0.6 eV giving approximately a mobility gap of 1.0 eV - 1.1 eV.

In the temperature range between $400^{\circ}K$ and $289^{\circ}K$ the dominant conduction mechanism is different. In this temperatur range electrons jump to tail states closer to the conduction band.

At temperatures between $289^{\circ}K$ to $200^{\circ}K$, the conductivity mechanism involved is hopping conduction between the nearest neighbours around the Fermi level.

In the low temperature range, below $200^{\circ}K$ and at small electric fields between $10^2$ - $10^3$ V/cm, the conductivity of these films obey the $T^{-1/4}$ law as proposed by Mott. These low temperature variable range hopping measurement results are then used to calculate the density of states around the Fermi level which gives a value of the order of $\sim 10^{18}$ $(cm^3 - eV)^{-1}$. The results show that the density of dangling

bonds in these films is similar to those prepared by rf sputtering and much higher than those prepared by glow-discharge decomposition of silane ($SiH_4$).

AC measurements using small electric fields have also the advantage that effects such as field assisted tunneling are avoided. For this reason we have used amplitudes of 1.1 - 0.7V.

We tried to interpret our experimental AC results according to the quantum-mechanical tunneling model (Austin-Mott), predicted to be of the form,

$$\sigma(\omega) = A\omega \ln^4 (\nu_{ph}/\omega)$$

which for constant $\nu_{ph}$, has the form,

$$\sigma(\omega) = A\omega^s$$

with s independent of temperature in a certain temperature range. Experimental results have shown that s is temperature dependent above approximately 160°K.

The Austin-Mott formula(Eq. 1.7) predicts s values of 0.83 to 0.75 from 100 Hz to $10^5$ Hz respectively. Experimental errors such as stray capacitances and lead resistances affect this theoretical value. Our s value is nearly in agreement with the value of 0.87. Other workers have obtained similar s values varying from unity to 0.5.

It is also necessary to realize that at low frequencies and high temperatures a departure from the relation $A\omega^s$ occurs for the following reason: The magnitude of $A\omega^s$ falls below the DC conductivity. This is ascribed to a

quite different mode of conduction, namely, transport by carriers excited into the conduction band. The frequency dependence of this mode of conduction is expected to be very small unless the excited carriers move by hopping between localized states in the conduction band edge. In this latter case a dependence on frequency is expected, but the process should be easily distinguishable from the band edge hopping, which has an activation energy equal to roughly half the bandgap.

# REFERENCES


1. Mott, N.F. and Davis, E.A., Electronic Processes in Non-Crystalline Materials. Oxford: Clarenden Press, 1979.

2. Atağ, Y., " Study of the DC Conductance Mechanism of Evaporated Amorphous Silicon Films, " M.S. Thesis, Boğaziçi University, 1984.

3. Elliott, S.R., "Defect States in Amorphous Silicon, " Philosophical Magazine B, Vol. 38, No. 4, pp. 325-334, 1978.

4. Spear, W.E. and Le Comber, P.G., " Investigation of the Localized State Distribution in Amorphous Silicon Films, " Journal of Non-Crys. Solids, Vol. 8-10, pp. 727-738, 1972.

5. Cohen, M.H., Fritzche, H. and Ovshinsky, S.K., " Simple Band Model for Amorphous Semiconducting Alloys, " Phys. Rev. Letters, Vol. 22, No. 2, pp. 1065-1068, 1969.

6. LeComber, P.G., Electronic and Structural Properties of Amorphous Semiconductors, London: Academic Press, 1972.

7. Aktaş, G. and Skarlatos, Y., " Determination of the Gap Density of States in Amorphous Silicon by Phase Shift Analysis of the Modulated Photocurrent, " J. Appl. Phys, Vol. 55, No. 10, 1984.

8. Abkowitz, M., Le Comber, P.G. and Spear, W.E., " AC Conductivity in Amorphous Silicon and Germanium and the Density of states at the Fermi Level, " Comm. Phys, Vol. 1, pp. 175-182, 1976.

9. Brodsky, M.H. Amorphous Semiconductors. Springer-Verlag, Berlin, 1979.

10. Guha, S. and Narasimhan, L., " On Variable Range Hopping in Amorphous Films of Germanium and Silicon, " Thin Solid Films, Vol. 50, pp. 151-155, 1978.

11. Jonscher, A.K., " Frequency-Dependence of Conductivity in Hopping Systems, " Journal of Non-Crystalline Solids, Vol. 8-10, pp. 293-315, 1972.

12. Elliott, S.R., " A Theory of AC conduction in Chalcogenide Glasses," Phil. Mag, Vol. 36, No. 6, pp. 1291-1304, 1977.

13. Freeman, E.C. and Paul, P., " Optical Constants of rf-Sputtered Hydroganated Amorphous Silicon, " Phys. Rev. B, Vol. 20, pp. 716-728, 1979.

14. Chick, K.P. and Koon, K.C., " Evidence for Nearest-Neighbour Hopping in Amorphous Silicon, " Phil. Mag. B, Vol. 53, No. 5, pp. 399-405, 1986.

15. Davis, E.A. and Shaw, R.F., " Characteristic Phenomena in Amorphous Semiconductors, " J.Non-Crys. Solids, Vol. 2, pp. 406-431, 1970.

16. Elliott, S.R., " The Mechanism for AC Conduction in Chalcogenide Semiconductors: Electronic or Ionic, " Phil. Mag.B, Vol. 40, No. 6, pp. 507-511, 1979.

17. Long, A.R. and Balkan, N., " AC Loss in Amorphous Ge, " Phil. Mag.B, Vol. 41, No. 3, pp. 287-305, 1980.

18. Balkan, N., Butcher, P.N., Hogg, W.R., Long, A.R. and Summerfield, S., " Analysis of Frequency Dependent Loss Data in Amorphous Silicon and Germanium, " Phil.Mag.B, Vol. 51, No. 1, pp. L7-L12, 1985.

19. Wong, S.K., Tong, B.Y. and John, P.K., " High Stable Photosensitive Evaporated Silicon Films, " Appl. Phys. Letter, Vol. 30, No. 10, 1981.

20. Dey, S.K. and Tong, B.Y., " Conduction Processes and Threshold Switching in Amorphous Silicon Films, " J. Vac. Sci. Technology, Vol. 16, No. 2, pp. 240-243, 1979.

21. Dellaferra, P., Labush, R. and Roscher, H.H., " An Alternative Method of Preparing Hydrogen Doped Evaporated Amorphous Silicon, " Phil. Mag.B, Vol. 43, No. 1, pp. 169-172, 1981.